ACS OMEGA

http://pubs.acs.org/journal/acsodf

Article

Electron Transport of the Nanojunctions of $(BN)_n$ (n = 1−4) Linear Chains: A First-Principles Study

Ying-Qin Zhao, Jun-Qing Lan, Cui-E Hu,* Yi Mu,* and Xiang-Rong Chen*

Cite This: *ACS Omega* 2021, 6, 15727−15736

Read Online

ACCESS | Metrics & More | Article Recommendations

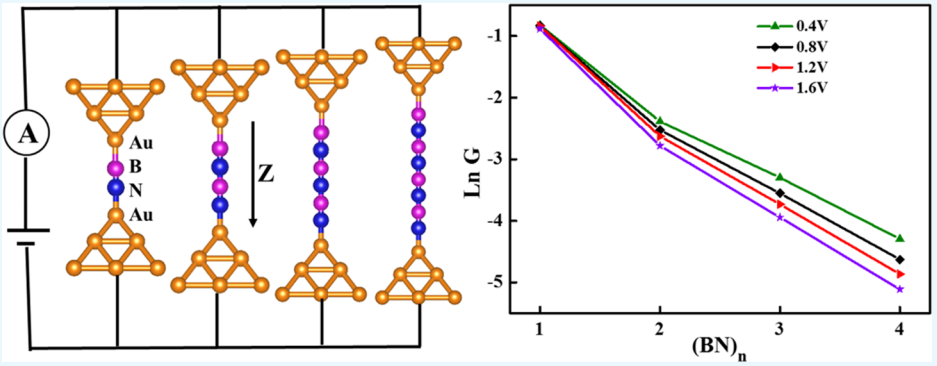

ABSTRACT: We applied the density functional theory and nonequilibrium Green's function method (DFT + NEGF) to investigate the relationship between the conductance and chain length in the stretching process, the asymmetric coupling of contact points, and the influence of positive and negative biases on the electron transport properties of the nanojunctions formed by the coupling of $(BN)_n$ (n = 1−4) linear chains and Au(100)-3 × 3 semi-infinite electrodes. We find that the BN junction has the lowest stability and the $(BN)_2$ junction has the highest stability. Under zero bias, the equilibrium conductance decreases as the chain length increases; p_x and p_y orbitals play a leading role in electron transport. In the bias range of −1.6 to 1.6 V, the current of the $(BN)_n$ (n = 1−4) linear chains increases linearly with increasing voltage. Under the same bias voltage, $(BN)_1$ has the largest current, so its electron transport property is the best. The rectification effect reflects the asymmetry of the structure of BN linear chains themselves and the asymmetry of coupling with the Au electrode surfaces at both ends. With the chain length increasing, the transmission spectrum near E_f is suppressed, the tunneling current decreases, and the rectification ratio increases. $(BN)_4$ molecular junctions have the largest rectification ratio, reaching 13.32 when the bias voltage is 1.6 V. Additionally, the Au−N strong coupling is more conducive to the electron transport of the molecular chain than the Au−B weak coupling. Our calculations provide an important theoretical reference for the design and development of BN linear-chain nanodevices.

INTRODUCTION

With the continuous innovation and improvement in technology of manipulating semiconductor nanodevices, the miniaturization of electronic components has become the current frontier of nanoresearch. Among many candidates, one-dimensional (1D) nanostructures, such as nanowires, nanochains, and nanotubes, are considered to be the final quantum conductors, and they can be used as components or nanoconnections of nanoelectronic devices in the future.[1,2] Their mechanical, optical, and electronic properties have been extensively studied.[3−5] The limit model of a one-dimensional conductor is the atomic chain. Experimental methods such as scanning tunneling microscopy (STM)[6] and the mechanically controllable break junction technique (MCBJ)[7] make it possible to synthesize and manipulate monoatomic chains.

In 1998, Ohnish et al.[8] and Yanson[8,9] made breakthrough progress using STM and MCBJ techniques: A stable gold monatomic chain was made and suspended between two Au electrodes. Subsequently, C,[10−12] Si,[13] S,[14] and other atomic chains are formed. Many novel properties of atomic chains, such as conductance quantization and even−odd conductance oscillations, have been discovered.[8,15−18] Due to the potential of atomic chains in miniaturization and multifunction of electronic devices, the electron transport properties of atomic nodes have attracted the interest of many researchers in experiments and theoretical calculations.[19] For example,

Received: February 23, 2021
Accepted: May 31, 2021
Published: June 8, 2021

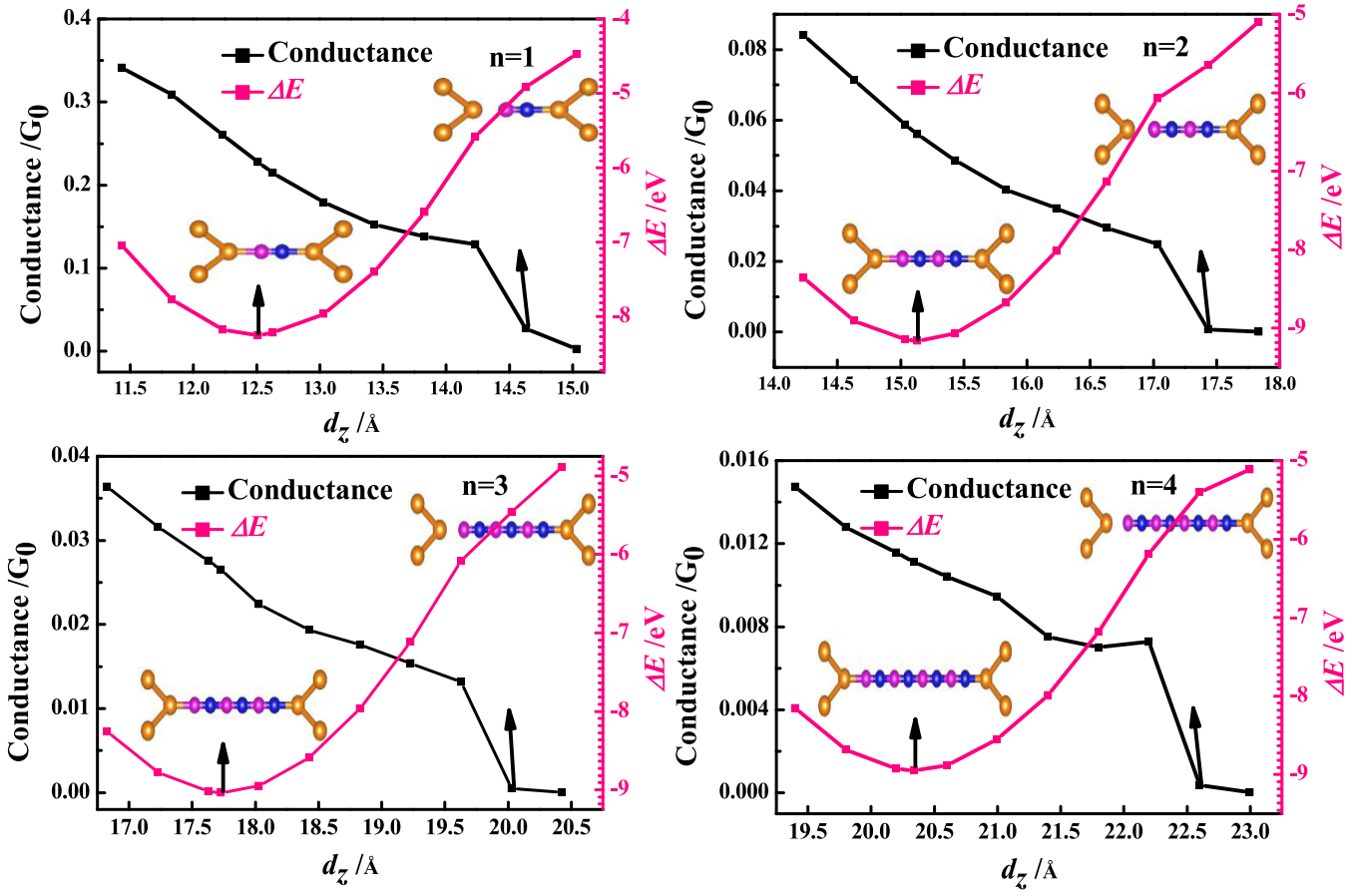

Figure 1. Relationship between binding energy ΔE (eV) and conductance G (G_0) with distance d_z (Å). ΔE represented by a red solid line, and the ordinate corresponds to the right axis. G is represented by a black solid line, and the ordinate corresponds to the left axis.

Lang[20] first studied the relationship between the conductance of the Na atomic wire connected to the two electrodes and the number of atoms and found that as the length of the atomic chain changes, the conductance of the atomic wire oscillates with a period of two atoms. This phenomenon is also found in the atomic chains of Au, Pt, Ir, Al, and so on.[21−25] In addition to metal atomic chains, the chains of semiconductor or insulator materials have been extensively studied as well. There are related reports on the conductance of monatomic chains of C, Si, S, Ge, and Sn and binary compound molecular chains, such as InP, GaAs, AlSb, SiC, GaN, and AlN.[26−28]

As an important III−V group inorganic nonmetallic material, BN has a series of excellent physical and chemical properties and has potential applications in many aspects. With the continuous in-depth research on materials, the theoretical research and preparation technique of BN nanomaterials have also been vigorously developed. At present, in experiments, one-dimensional boron nitride nanowires (BNNWs) have been successfully synthesized.[29,30] BN chains have been fabricated by irradiating h-BN sheets with electron beams.[31,32] In terms of theory, Zhang et al.[33] constructed a series of periodic three-dimensional (3D) stereoscopic BN molecular structures and named them T-B_xN_x ($x = 4n - 1$, n = 1, 2, 3, ...); they calculated the electronic structures of these BN molecules based on the density functional theory (DFT) method through the VASP software package. Their results showed that these molecular structures composed entirely of nonmetallic atoms exhibit strong metallic properties. Based on the interest in these T-B_xN_x molecular units with novel properties, Wang et al.[34,35] constructed several 3D structures of BN molecular junctions and studied their electron transport properties. Furthermore, Zeng et al.[36] studied the electron transport properties of BN chains between two-dimensional (2D) metallic boron−benzene electrodes by nonequilibrium Green's function. They found that when the BN chain was coupled to 2D borophene electrodes, it showed metallic characteristics, and its negative differential resistance (NDR) behavior was observed. Meanwhile, Xu et al.[37] showed that the BN linear chain has a rectification effect and negative differential resistance. However, the relationship between the conductance and chain length, the mechanical and electrical properties of molecular junctions in the stretching process, the asymmetric coupling of contact points, and the influence of positive and negative biases on the electron transport properties need to be further understood. Therefore, we believe that the theoretical simulation of the electron transport behavior of the linear BN molecular chain is very important for predicting or explaining the available experimental results.

In this work, by applying the DFT[38] and nonequilibrium Green's function (NEGF) method,[39] we have systematically studied the influence of chain length, the unequal contact on the conductivity, and the $I-V$ characteristics of the BN linear chain sandwiched between Au electrodes. We have simulated the rupture processes of Au-$(BN)_n$ (n = 1−4)-Au junctions and calculated the $I-V$ characteristics at the equilibrium position. It is found that, in the bias range of −1.6 to 1.6 V, the current of the $(BN)_n$ (n = 1−4) linear chains increases with increasing voltage.

https://doi.org/10.1021/acsomega.1c00999
ACS Omega 2021, 6, 15727−15736

Table 1. Optimized Bond Lengths (Å) for $(BN)_n$ (n = 1−4) Linear Chain Suspended between Au Electrodes

n	Au-B1	B1-N2	N2-B3	B3-N4	N4-B5	B5-N6	N6-B7	B7-N8	N8-Au	R_{BNav}
1	2.003	1.267							1.932	1.267
2	2.002	1.271	1.350	1.272					1.918	1.298
3	1.993	1.277	1.333	1.278	1.341	1.279			1. 913	1.302
4	1.989	1.282	1.327	1.284	1.326	1.282	1.337	1.282	1.911	1.303
cal.										1.300[44−46]
exp.										1.31[31]

RESULTS AND DISCUSSION

Simulation of the Stretching Process. Since the $(BN)_n$ (n = 1−4) linear chain is connected to the two semi-infinite Au electrodes to form nanoscale junctions, the atomic interaction at the interface coupling will change, which will inevitably lead to a change in the structure of the junction. Therefore, the junction structure should be geometrically optimized before calculating the electronic transport. Taking into account the electrostatic shielding effect of the electrode, when the structure is optimized, all of the atoms of the electrodes are fixed except for the 1−2 atomic layers near the interface, so that the atoms between the two-pyramid bottoms can be fully relaxed and find their respective equilibrium positions. The distance between two-pyramid bottoms is defined as d_z (as shown in Figure 9), and the binding energy of the junction is $\Delta E = E$ [Au-$(BN)_n$-Au]−E(Au leads)−E[$(BN)_n$]. The calculated relationship between ΔE of each junction and d_z is shown in Figure 1. In the figure, ΔE is represented by a red solid line and the ordinate corresponds to the right axis.

The curves of ΔE versus d_z for all structures present a parabolic shape, which means that they all have the most stable equilibrium structure. For $(BN)_n$ (n = 1−4) linear chains, their equilibrium distances are d_z = 12.631, 15.134, 17.728, and 20.598 Å for each n, respectively; the corresponding ΔE values of the junctions are −8.311, −9.161, −9.035, and −8.948 eV, showing that BN has the lowest stability and $(BN)_2$ has the highest stability. For $(BN)_{2\text{-}4}$, the molecular chain length increases and the stability of the system decreases. The calculated results of the bond lengths of B−N, Au−B, and Au−N for each equilibrium structure are shown in Table 1. It is observed from Table 1 that the characteristics of the bond length oscillation are similar to the carbon atom chains with different lengths and terminations.[40−43] The average bond lengths of the B−N bonds are 1.267, 1.298, 1.302, and 1.303 Å, respectively, which are in good agreement with the theoretical and experimental results (1.300 and 1.310 Å)[31,44−46] as the length increases. It can be seen from Table 1 that the optimized structures are almost symmetric about the center of the molecular chain, which is similar to the covalent coupling of the carbon monoatomic chain with Au electrodes.[47,48] Also, the short and long B−N bonds alternatively appear in the linear chains. As n enlarges, short bonds become longer and long bonds become shorter. This change is the result of different types of hybridization between the electronic states of the linear chains of different lengths and the electrode surface states.[49]

We calculated the conductance of each molecular chain at different distances d_z and obtained the result of the change of conductance G with d_z, as also shown in Figure 1. G is represented by a black solid line, and ΔE corresponds to the left axis. It can be seen from Figure 1 that the variation of d_z is less than 4 Å which is very small (<1 nm). However, with an increase of d_z, the conductance value of the nanojunction changes significantly. It indicates that the distance d_z between the two electrodes is an important factor affecting the conductance of the structure. In other words, local atomic rearrangements have a great influence on the conductance of the junctions.[50,51] This is exactly the physical mechanism of the extremely high resolution of an electron scanning tunneling microscope. We noticed that the conductivity decreases with an increase of d_z. When d_z increases by 3.2 Å, the conductance suddenly decreases; at this time, the Au−B bond has been broken. When each junction of Au−$(BN)_n$−Au is in a stable equilibrium structure, the equilibrium conductances under zero-bias voltage are 0.228, 0.056, 0.027, and 0.011 G_0. As the length of the linear chain increases, the conductivity reduces to almost half of the former. The decrease should be attributed to the weakening of hybridization at the molecular−electrode contact point when the molecular chain becomes longer. We did not find the even−odd conductance oscillations, and this phenomenon is not found in other linear chains.[28,37,52,53] The difference may be due to the different electrodes and geometric configurations used.

Many studies have shown that when the distance d between two electrodes is less than 5 nm, the conductance decreases exponentially with an increase of d, namely, $G = G_0 e^{-\beta d}$, where β is the attenuation factor.[54−61] The value of β largely depends on the type of molecule. It is generally considered that $\beta \sim 0.2$ to 0.3 Å^{-1} for conjugated molecules[54,55,58] and 0.5−1 Å^{-1} for saturated molecules;[57] there are also some molecular systems with β values below 0.1 Å^{-1}.[56,59−61,56,59−61] We calculate the β of $(BN)_{n\,=\,1-4}$ linear molecular chains at equilibrium distances d_z under zero bias (see Figure 2); the value of β is 0.986 Å^{-1}, which is similar to the β values of saturated molecules.

Transmission Spectra and Density of States (DOS). We know that the properties of quantum transmission can be well

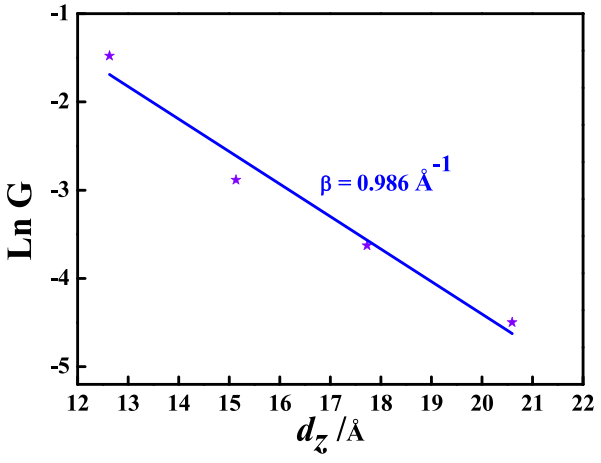

Figure 2. Attenuation factor β vs equilibrium distances d_z under zero bias for $(BN)_n$ (n = 1−4); β is the slope of the lines.

https://doi.org/10.1021/acsomega.1c00999
ACS Omega 2021, 6, 15727−15736

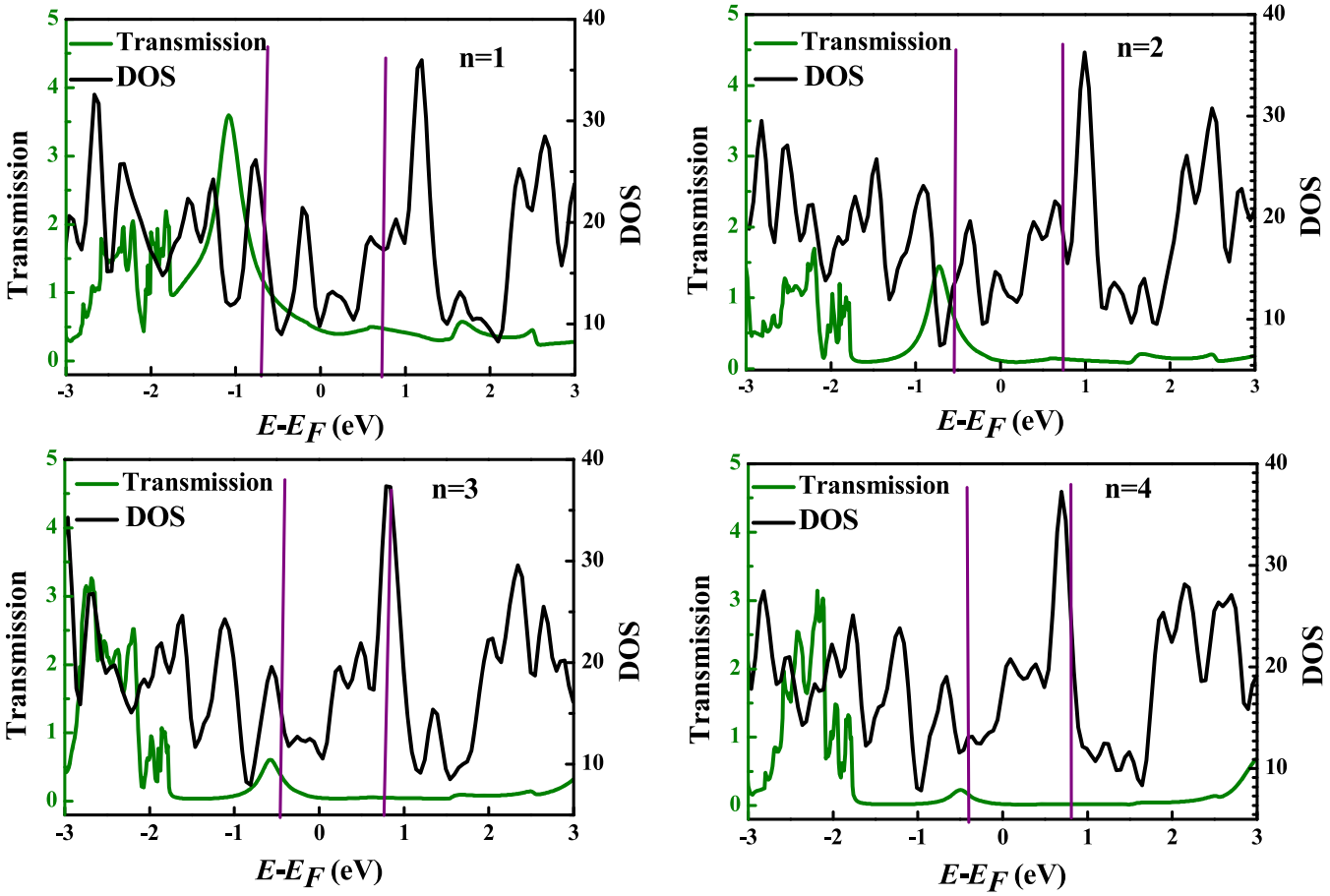

Figure 3. Transport coefficient and density of state as a function of energy for $(BN)_n$ (n = 1−4) linear chain at zero bias. The vertical lines stand for the molecular orbitals.

explained by the quantum transmission spectrum, which reflects the coupling strength between the system and the electrode, and the transmission channel implies the coupling strength between the molecular orbital and the electrode energy band.[62] To understand the relationship between the equilibrium conductance of the BN linear chain and the increase of the chain length in more detail, we figured out the relationship between the transmission coefficient of the $(BN)_{n=1-4}$ linear chains and the incident electron energy under zero bias, that is, the transmission spectrum $T(E, V = 0)$; the result is shown in Figure 3. It can be seen that the four systems have an obvious resonance peak near the Fermi level E_f, and the E_f is set to zero in this article. When more BN molecules are added to the molecular chain, more interactions between atoms cause more independent transmission peaks in the transmission spectra. The electron transmission characteristics mainly depend on the interaction between the frontier molecular orbital of energy near E_f and the electronic state of the electrode surface,[63] so we pay attention to the transmission spectrum near E_f. Obviously, the peak near E_f is greatly suppressed as the molecular chain becomes longer. Especially for the $(BN)_4$ molecular chain, the resonance peak near E_f is almost invisible, which proves that it is not conducive to electron transport. As a result, the equilibrium conductance of the BN molecular chain decreases as the chain length increases (as shown in Figure 1).

In fact, the peak value of the transmission spectrum is related to the molecular orbital of the BN linear chain. However, when the molecular chain is placed between the two electrodes to form a double-probe system, the molecular orbital energy level and spatial distribution of the linear chain will expand and move under the action of the Au electrodes,[64−66] and the transmission of electrons is carried out through these extended molecular orbitals. Therefore, it is necessary for us to consider the molecular orbital of the scattering region, that is, use the molecular projection self-consistent Hamiltonian (MPSH) method for orbital analysis.[64−66] It can be seen from the diagrams in Figure 5 that when the molecular chain becomes longer, the coupling between the chain and the electrodes decreases and the overlap between the MPSH state and the electrode surface state reduces, resulting in a narrower resonance peak and an increase in the number of resonance peaks, which is caused by more molecular eigenstates.[67] Electron transfer occurs mainly between the highest occupied molecular orbital (HOMO) and the lowest unoccupied molecular orbital (LUMO) during transport. It can be seen from Figure 3 that the HOMO level is closer to the Fermi level E_f than the LUMO level, so it plays a major role in electron transport. With an increase of BN molecular unit, the position of the HOMO-related resonance peak changes and the corresponding peak decreases, indicating that the MPSH eigenvalue, that is, the frontier molecular orbital energy level, is very sensitive to the length of the molecular chain. When n increased from 1 to 4, the HOMO−LUMO gaps become smaller, which are 1.461, 1.438, 1.315, and 1.248 eV, respectively; these gaps are smaller than the

https://doi.org/10.1021/acsomega.1c00999
ACS Omega 2021, 6, 15727−15736

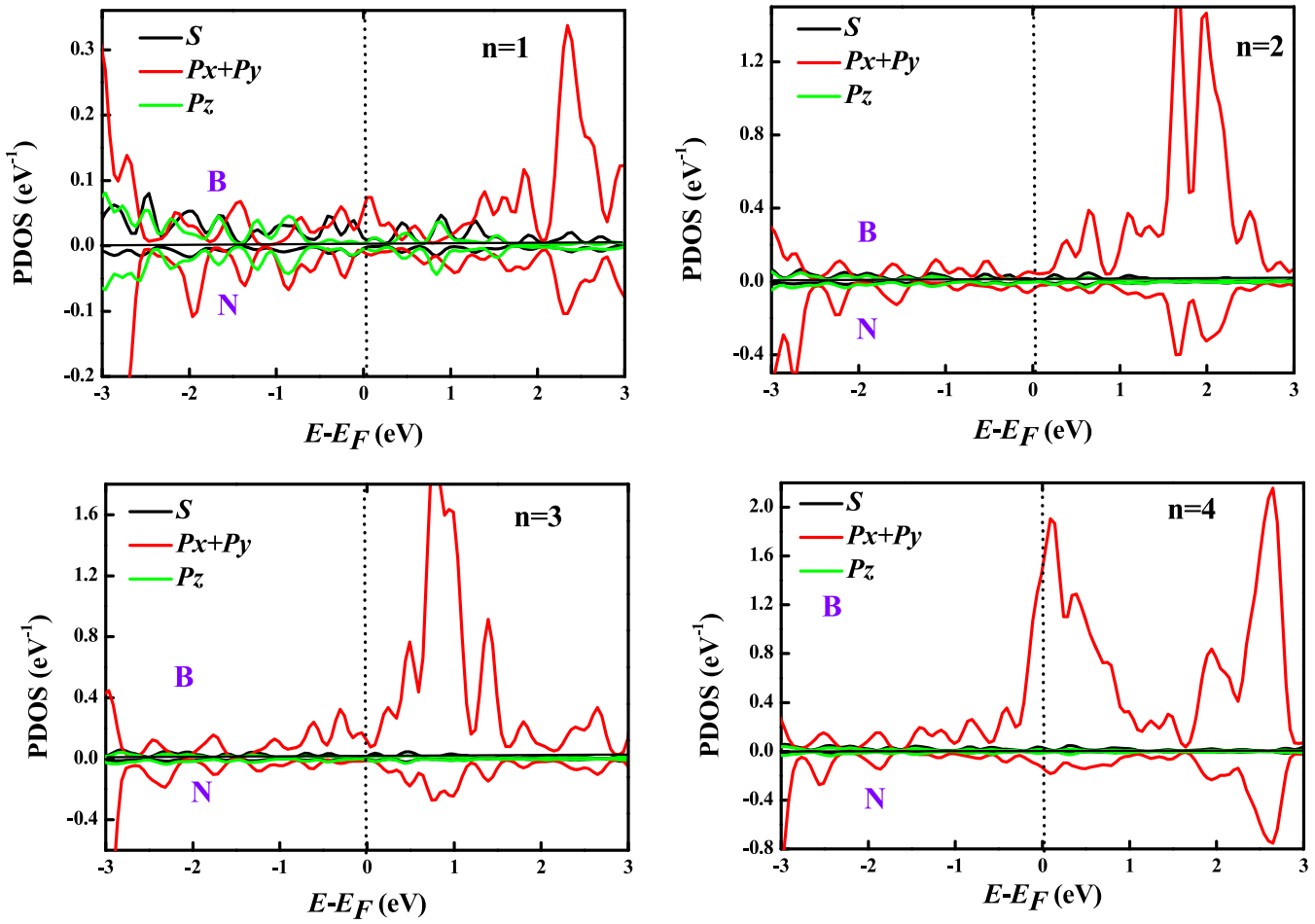

Figure 4. Projected density of states of the $(BN)_n$ (n = 1−4) linear chains under zero external bias.

MPSH	HOMO-1	HOMO	LUMO	LUMO+1
n=1	-0.776eV	-0.761eV	0.700eV	1.335 eV
n=2	-0.752eV	-0.649eV	0.789eV	1.137 eV
n=3	-0.734eV	-0.509eV	0.806eV	1.082 eV
n=4	-0.726eV	-0.435eV	0.813eV	1.046 eV

Figure 5. Spatial distribution of MPSH orbitals near the Fermi level E_f of $(BN)_n$ (n = 1−4) linear chains at zero bias. The isovalue is set to 0.04 for all plots.

value of polyyne-based molecular wires calculated by Crljen[49] and larger than the gaps of the SiC chains calculated by Mu et al.[68] We also calculated the gaps when the $(BN)_{1-4}$ linear chains are not connected to the electrodes; they are 9.000, 7.020, 5.882, and 4.973 eV, respectively. It can be seen that the connection of $(BN)_{1-4}$ linear chains to the electrodes greatly reduces the energy gap.

To better understand the transport channel, we further analyze the density of states (DOS) of the molecular chains, as shown in Figure 3. The vertical dashed lines represent the molecular orbitals. All molecular orbitals near the E_f can promote electron transport. If an orbital delocalizes on the entire molecule, the electrons that reach the molecule with the energy of the delocalized orbital have high mobility. In this

https://doi.org/10.1021/acsomega.1c00999
ACS Omega 2021, 6, 15727−15736

case, it corresponds to a certain peak of the transmission spectrum. In general, the number of discrete peaks in the DOS diagram corresponds to the different molecular orbitals of the linear chain, and the molecular orbitals correspond to energy-independent transport coefficients; therefore, the peak value in the DOS diagram has a good corresponding relationship with the peak value in the transport coefficient. We can see from the figure that although new molecular orbitals are added, the characteristic spectra of the molecular chains do not move to the E_f and the transmission coefficients are suppressed with an increase of the chain length, so the conductance decreases. We also analyze the projected density of states (PDOS) of the molecular chains, as shown in Figure 4. The p_x and p_y orbitals of the B atom and N atom show a high density of states near E_f. Therefore, the p_x and p_y orbitals make major contributions to the transport channel, forming a π bond that is beneficial to electron transport, but the s and p_z orbitals have a little contribution.

MPSH Eigenstates. The spatial distribution of frontier molecular orbitals can be used to qualitatively understand the contribution of molecular orbitals in the transport process and the coupling between the molecular chains and the electrodes at both ends.[69−71] Since the orbitals near E_f play a dominant role in transport, Figure 5 lists the spatial distribution of MPSH orbits near E_f and the corresponding MPSH eigenvalues under zero bias. We found that although the lengths of the molecular chains are different, the spatial distribution of the HOMO and LUMO of the frontier orbitals are similar. Combining Figures 3 and 5, it can be seen that LUMO and LUMO + 1 orbitals of $(BN)_1$ play a decisive role in electron transport, the HOMO resonance states of the $(BN)_n$ (n = 2−4) molecular chains correspond to the transmission spectrum peak, and their orbital spatial distributions are more delocalized than LUMO, LUMO + 1, and HOMO − 1, so the HOMO orbitals provide a good transmission channel for charge transport. At the corresponding energy of LUMO, the electron transmission probability is obviously lower. The spatial distribution domain of the orbital is on the Au atom on the electrode side, and as the chain length increase, the distribution on the intermediate molecular chains becomes less and less. Therefore, the LUMO orbitals contribute less to the conductances of the molecular junctions. As the length of the molecular chain increases, the degree of delocalization of the orbital decreases, and the HOMO resonance is severely deformed and strongly suppressed, which leads to a decrease of the conductance of BN linear chains. In addition, as the length of the molecular chains increases, HOMO changes from a nondegenerate state at n = 1 to a degenerate state at n = 2−4, which means that increasing the chain length can degenerate the system.

By analyzing the spatial distribution of MPSH orbitals, information about the coupling of molecular chains and electrodes during the formation of molecular junctions can also be obtained. In the HOMO state, as n = 1 extends to n = 4, the coupling between the molecular chains and the left electrode is significantly weakened, and at the contact point between the molecular chains and the right electrode, the orbital always maintains a relatively delocalized spatial distribution, which means that the coupling between the molecular chains and the right electrode is stronger than the coupling with the left electrode, which has an important effect on electron tunneling between the chains and the electrodes, similar to the calculation results of Xu et al.[37] The overlap of Au−N electronic states is greater than Au−B electronic states; this conclusion can be verified by the fracture of the Au−B bond during the stretching process, as shown in Figure 1.

I−V Characteristic Curves and Rectification. The external bias will cause the Hamiltonian of the electrodes to move, and the chemical potential of the electrodes changes to generate current. Figure 6 shows the junction current under a region from −1.6 to 1.6 V.

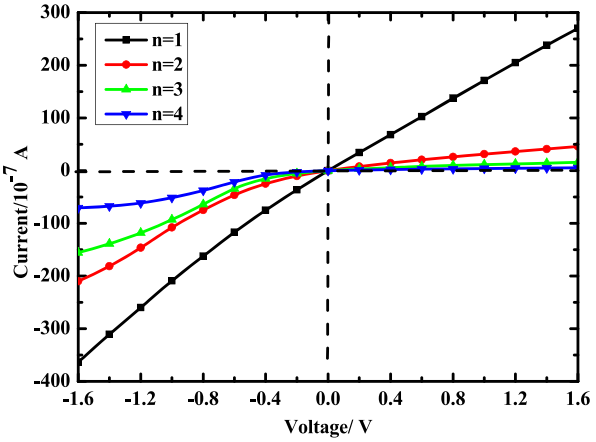

Figure 6. Current as a function of the applied bias for the $(BN)_n$ (n = 1−4) linear chain.

We found that the chain length has a great influence on the characteristics of the $I-V$ curves. The $I-V$ curves of the $(BN)_n$(n = 1−4) nanojunctions show nearly linear changes in the entire bias voltage range. For n = 1 molecular junction, the current increases rapidly with an increase of the bias voltage. This is due to the interaction between the chain and the metal electrodes, resulting in electrons of metal doped into the BN line chins. Under the positive bias, the currents increase slowly, particularly the currents of $(BN)_{2\text{-}4}$ chains hardly change with the voltages. Under the negative bias, the current increases apparently as the chain grows. Also, as the lengths of the molecular chains increase, the currents decrease. Figure 6 also shows that the magnitude of current flowing through the $(BN)_1$ chain is much greater than that flowing through the $(BN)_{2\text{-}4}$ chains under the positive voltage. In addition, it can be seen from Figure 6 that the $I-V$ curves of the BN linear chains exhibit asymmetric characteristics. On the one hand, this asymmetric characteristic is derived from the asymmetry of the molecular chains themselves; on the other hand, it stems from the asymmetry of the contact between the molecular chains and the electrodes.[66] The asymmetry of the current can be quantified by the reverse rectification ratio of the molecular junction changing with the bias voltage, which is defined as follows:[72] $R(V) = |(I(-V)/I(V)|$. Figure 7 shows the change curves of the rectification ratios of the molecular chains with the bias voltages. It can be seen that for all of the $(BN)_n$ (n = 1−4) linear chains, the reverse rectification ratios are greater than 1, which indicate that the currents under the negative bias are greater than those under the positive bias, and the rectification ratio is related to the length of the molecular chain. As the molecular chains become longer, the rectification effect is significantly enhanced. For n = 4, the rectification ratio reaches the largest 13.32 at 1.6 V for all of the four molecular junctions; the ratio is similar to that of $(BN)_{5\text{-}8}$ studied by Xu et al.[37] and rather small compared to recent results of 6.3×10^5

https://doi.org/10.1021/acsomega.1c00999
ACS Omega 2021, 6, 15727−15736

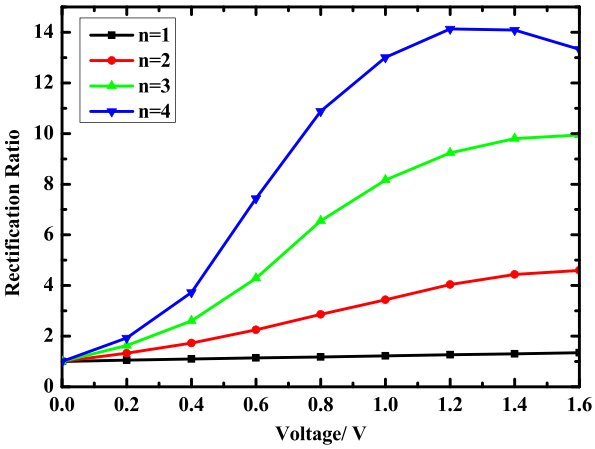

Figure 7. Rectification ratios as a function of the applied bias for the $(BN)_n$ (n = 1−4) linear chain.

of Fc−C≡C−Fc and above 1000 at low voltage[70,73] in oligo(bisthienylbenzene)-based layer systems.

It is worth noting that the characteristics of the volt−ampere curves of $(BN)_n$ (n = 1−4) molecular chains are quite different from those of Si single-atom chains[74] and C-atom chains with benzene rings,[75] and the negative differential resistance (NDR) effect, which exists in other BN molecular chain systems,[36,37] is not found in our $(BN)_n$ (n = 1−4) linear-chain systems. We took $(BN)_{2\text{-}3}$ junctions as an example to explain the transmission spectra under different bias voltages, as shown in Figure 8. From the Results and Discussion section, we know that at a certain voltage V, the current I through the junction is determined by the integral of the transmission coefficient T within the energy window $[-eV/2, +eV/2]$, and the bias window is marked with the vertical dotted line. In the voltage range of −1.6 to 1.6 V, although the shape of the transmission spectrum does not change significantly, the HOMO peak gradually shifts to E_f and the bias window becomes broader with the increase of the bias; therefore, the current will increase with an increase of voltage under both positive and negative voltages, that is, in the range of −1.6 to 1.6 V, the nanojunctions of $(BN)_n$ (n = 1−4) molecular chains show no NDR behavior.

CONCLUSIONS

By first-principles density functional theory and nonequilibrium Green's function method, we systematically study the electron transport properties of Au-$(BN)_n$-Au nanojunctions formed by coupling of $(BN)_n$ (n = 1−4) linear chains with Au(100)-3 × 3 half-infinite electrodes. The influence of chain length on conductance, the asymmetry of the molecular chains and its coupling with the electrodes, and positive and negative biases on the electron transport characteristics is mainly discussed. When each junction is in an equilibrium structure, their equilibrium distances are d_z = 12.631, 15.134, 17.728, and 20.598 Å, respectively; the corresponding ΔE values are −8.311, −9.161, −9.035, and −8.948 eV. It is found that the BN junction has the lowest stability and the $(BN)_2$ junction has the highest stability. For $(BN)_{2\text{-}4}$ nanojunctions, as the molecular chain length increases, the stability of the system decreases. The average bond lengths of B−N are 1.267, 1.298, 1.302, and 1.303 Å, and their equilibrium conductance under zero-bias voltages are 0.228, 0.056, 0.027, and 0.011 G_0, respectively.

Under zero bias, the p_x and p_y orbitals contribute the most during the transportation process and play a leading role in electron transport. As the chain length increases, the transmission spectrum near E_f is suppressed, the tunneling current decreases, and the rectification ratio increases. The I−V curves of the $(BN)_n$(n = 1−4) nanojunctions show nearly linear changes over the entire bias voltage range. Under the same voltage, $(BN)_1$ has the largest current, and its electronic transport is the best. The rectification effect reflects the asymmetry of the structure of BN linear chains themselves and the asymmetry of the coupling with the Au electrode surfaces at both ends. Among the four molecular junctions, $(BN)_4$ has the largest rectification ratio, reaching 13.32 when the bias voltage is 1.6 V. The Au−N strong coupling is more conducive to the electron transport of the molecular chain than the Au−B weak coupling. Our calculations provide a systematic and comprehensive study on the electronic transport characteristics of BN linear chains and we hope to provide an important theoretical reference for the design and development of BN nanodevices.

COMPUTATIONAL DETAILS

To calculate the electron transport properties of the $(BN)_n$ (n = 1−4) linear chain, the two-end device model of electron transport in a typical mesoscopic system is used to connect the molecular chain and the electrode to form a nanojunction.[7] A certain voltage is applied to the terminal to measure the current through the node. To ignore the influence of the interface on the electron transport properties of the molecular chain, the coupling morphology of the chain and the electrode

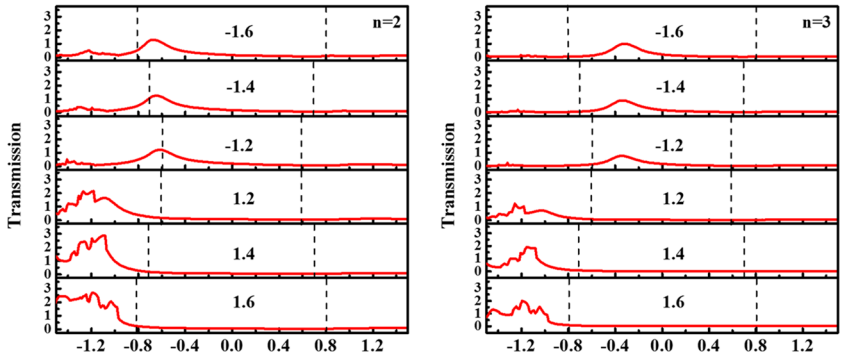

Figure 8. Transmission spectra of $(BN)_{(2\text{-}3)}$ molecular chains under bias voltage ±1.2, ±1.4, and ±1.6 V. The vertical dashed lines represent the bias window.

https://doi.org/10.1021/acsomega.1c00999
ACS Omega 2021, 6, 15727−15736

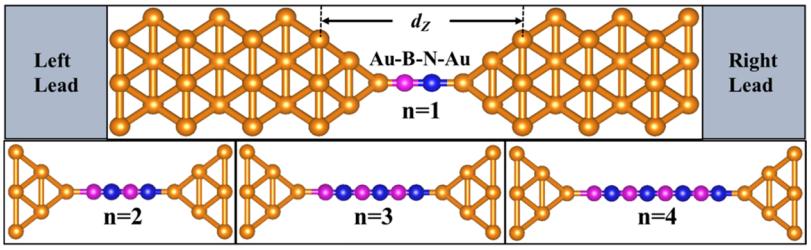

Figure 9. Model diagram of the $(BN)_n$ (n = 1−4) linear chains sandwiched between two Au(100) electrodes.

is controlled, and a pyramid structure is added at the coupling point to connect the BN chain to the top position of the atom at the tip of the electrode. In Figure 9, we illustrate the model diagram of the $(BN)_n$ (n = 1−4) linear chains sandwiched between two Au (100) electrodes. The model can be divided into three parts, the left electrode, the central scattering area, and the right electrode, and proved to be reliable.[68,76] The electrode can be treated with a semi-infinite ideal metal crystal structure. Because Ke et al.[77] found that under low voltages, the electron transport characteristics given by the finite interface Au electrode and the periodic three-dimensional body electrode, especially in the (100) direction, are almost identical. To avoid the interaction between mirror image molecules, a 3 × 3 supercell structure is used in the vertical direction, so in this paper, two half-infinite Au(100)-3 × 3 × 2 unit cells are selected as electrodes. To shield the interaction between the linear chain and the electrode, the BN linear chain and other Au tips with 7(6) Au layers on the left(right) constitute the central scattering zone.[78] The electron transport direction is from the left to right.

In theoretical simulation calculations, the nonlocal norm-conserving Troullier−Martins pseudopotential[79] is used to describe the core electrons, and the valence electrons of Au atoms use a single-ζ polarized (SZP) basis set, while double-ζ polarized (DZP) for B and N. The energy convergence standard for self-consistent calculation is 10^{-4}, and the cutoff energy is 300 Ry. A 2 × 2 × 100 k-point grid is taken perpendicular to the electron transport direction. The exchange−correlation function selects the Perdew−Zunger form[80] of the local density approximation (LDA-PZ),[81] which has been proven reasonable and reliable.[36,80,82] The calculation of the electronic transport properties of the $(BN)_n$ (n = 1−4) linear chain is done by the SIESTA program[83] based on DFT.[84] The SIESTA calculation software package has been successfully applied to various models, and the good results consistent with experiments and other ab initio calculations make us confident in the reliability of the calculations.[41,84−86] The calculation of electronic transport characteristics adopts the TRANSIESTA program, which is a module of SIESTA based on the NEGF technique.[83] In the transportation calculation, the charge density is integrated over 50 energy points along the semicircle on the complex plane, 20 energy integration points are selected on the imaginary axis, and 20 poles are used for the Fermi distribution function.

When a certain external voltage is applied to both ends, the current through the node can be obtained by the following Landauer−Büttiker formula[86]

$$I(V) = \frac{2e}{h}\int T(E, V)[f(E-\mu_L) - f(E-\mu_R)]\mathrm{d}E \quad (1)$$

In the formula, f is the Fermi distribution function, $\mu_{L/R}$ is the chemical potential of the left and right electrodes, and $T(E, V)$ is the transmission coefficient of electrons with energy E from the left electrode to the right electrode at voltage V. The integration interval is $[\mu_L, \mu_R]$, which is $[E_F - eV/2, E_F + eV/2]$. When the external bias voltage V = 0 V, the equilibrium conductance of the system can be obtained by multiplying the quantum conductance ($G_0 = 2e^2/h$) with the transmission value T (E_F, V = 0 V) at the Fermi level E_F in the equilibrium state, that is

$$G = \frac{2e^2}{h}T(E_F, V = 0\ V) \quad (2)$$

AUTHOR INFORMATION

Corresponding Authors

Cui-E Hu − *College of Physics and Electronic Engineering, Chongqing Normal University, Chongqing 400047, China*; Email: cuiehu@cqnu.edu.cn

Yi Mu − *School of Physics and Electronic Engineering, Sichuan Normal University, Chengdu 610066, China*; Email: muyichina@163.com

Xiang-Rong Chen − *College of Physics, Sichuan University, Chengdu 610064, China*; orcid.org/0000-0003-4528-2198; Email: xrchen@scu.edu.cn

Authors

Ying-Qin Zhao − *College of Physics, Sichuan University, Chengdu 610064, China*

Jun-Qing Lan − *College of Electronic Engineering, Chengdu University of Information Technology, Chengdu 610225, China*

Complete contact information is available at: https://pubs.acs.org/10.1021/acsomega.1c00999

Author Contributions

All authors listed have made a substantial, direct, and intellectual contribution to the work and have given approval to the final version of the manuscript.

Notes

The authors declare no competing financial interest.

ACKNOWLEDGMENTS

This work was supported by the National Natural Science Foundation of China (Grant No. 12074274) and the NSAF (Grant No. U1830101).

REFERENCES

(1) Yelin, T.; Vardimon, R.; Kuritz, N.; Korytar, R.; Bagrets, A.; Evers, F.; Kronik, L.; Tal, O. Atomically wired molecular junctions: connecting a single organic molecule by chains of metal atoms. *Nano Lett.* **2013**, *13*, 1956−1961.

(2) Guo, C.; Zhang, Z. H.; Kwong, G.; Pan, J. B.; Deng, X. Q.; Zhang, J. J. Enormously enhanced rectifying performances by

modification of carbon chains for D-sigma-A molecular devices. *J. Phys. Chem. C* **2012**, *116*, 12900−12905.
(3) Pham-Huu, C.; Keller, N.; Ehret, G.; Ledoux, M. J. The first preparation of silicon carbide nanotubes by shape memory synthesis and their catalytic potential. *J. Catal.* **2001**, *200*, 400−410.
(4) Wong, E. W.; Sheehan, P. E.; Lieber, C. M. Nanobeam mechanics: elasticity, strength, and toughness of nanorods and nanotubes. *Science* **1997**, *277*, 1971−1975.
(5) Seong, H. K.; Choi, H. J.; Lee, S. K.; Lee, J. I.; Choi, D. J. Optical and electrical transport properties in silicon carbide nanowires. *Appl. Phys. Lett.* **2004**, *85*, 1256−1258.
(6) Pomerantz, M.; Aviram, A.; Mccorkle, R. A.; Li, L.; Schrott, A. G. Rectification of stm current to graphite covered with phthalocyanine molecules. *Science* **1992**, *255*, 1115−1118.
(7) Reed, M. A.; Zhou, C.; Muller, C. J.; Burgin, T. P.; Tour, J. M. Conductance of a molecular junction. *Science* **1997**, *278*, 252−254.
(8) Ohnishi, H.; Kondo, Y.; Takayanagi, K. Quantized conductance through individual rows of suspended gold atoms. *Nature* **1998**, *395*, 780−783.
(9) Yanson, A. I.; Bollinger, G. R.; van den Brom, H. E.; Agrait, N.; van Ruitenbeek, J. M. Formation and manipulation of a metallic wire of single gold atoms. *Nature* **1998**, *395*, 783−785.
(10) Jin, C. H.; Lan, H. P.; Peng, L. M.; Suenaga, K.; Iijima, S. Deriving carbon atomic chains from graphene. *Phys. Rev. Lett.* **2009**, *102*, No. 205501.
(11) Cretu, O.; Botello-Mendez, A. R.; Janowska, I.; Cuong, P. H.; Charlier, J. C.; Banhart, F. Electrical transport measured in atomic carbon chains. *Nano Lett.* **2013**, *13*, 3487−3493.
(12) Andrade, N. F.; Aguiar, A. L.; Kim, Y. A.; Endo, M.; Freire, P. T. C.; Brunetto, G.; Galvao, D. S.; Dresselhaus, M. S.; Souza, A. G. Linear carbon chains under high-pressure conditions. *J. Phys. Chem. C* **2015**, *119*, 10669−10676.
(13) Bohloul, S.; Shi, Q.; Wolkow, R. A.; Guo, H. Quantum transport in gated dangling-bond atomic wires. *Nano Lett.* **2017**, *17*, 322−327.
(14) Fujimori, T.; Morelos-Gomez, A.; Zhu, Z.; Muramatsu, H.; Futamura, R.; Urita, K.; Terrones, M.; Hayashi, T.; Endo, M.; Hong, S. Y.; Choi, Y. C.; Tomanek, D.; Kaneko, K. Conducting linear chains of sulphur inside carbon nanotubes. *Nat. Commun.* **2013**, *4*, No. 2162.
(15) Hansen, K.; Laegsgaard, E.; Stensgaard, I.; Besenbacher, F. Quantized conductance in relays. *Phys. Rev. B* **1997**, *56*, 2208−2220.
(16) Smit, R. H. M.; Untiedt, C.; Rubio-Bollinger, G.; Segers, R. C.; van Ruitenbeek, J. M. Observation of a parity oscillation in the conductance of atomic wires. *Phys. Rev. Lett.* **2003**, *91*, No. 076805.
(17) Costa-Krämer, J. L. Conductance quantization at room temperature in magnetic and nonmagnetic metallic nanowires. *Phys. Rev. B* **1997**, *55*, R4875−R4878.
(18) Krans, J. M.; Vanruitenbeek, J. M.; Fisun, V. V.; Yanson, I. K.; Dejongh, L. J. The signature of conductance quantization in metallic point contacts. *Nature* **1995**, *375*, 767−769.
(19) Bahn, S. R.; Jacobsen, K. W. Chain formation of metal atoms. *Phys. Rev. Lett.* **2001**, *87*, No. 266101.
(20) Lang, N. D. Anomalous dependence of resistance on length in atomic wires. *Phys. Rev. Lett.* **1997**, *79*, 1357−1360.
(21) Lang, N. D.; Avouris, P. Oscillatory conductance of carbon-atom wires. *Phys. Rev. Lett.* **1998**, *81*, 3515−3518.
(22) Sørensen, M. R.; Brandbyge, M.; Jacobsen, K. W. Mechanical deformation of atomic-scale metallic contacts: Structure and mechanisms. *Phys. Rev. B* **1998**, *57*, 3283−3294.
(23) García-Suárez, V. M.; Rocha, A. R.; Bailey, S. W.; Lambert, C. J.; Sanvito, S.; Ferrer, J. Conductance oscillations in zigzag platinum chains. *Phys. Rev. Lett* **2005**, *95*, No. 256804.
(24) Thygesen, K. S.; Jacobsen, K. W. Four-atom period in the conductance of monatomic al wires. *Phys. Rev. Lett.* **2003**, *91*, No. 146801.
(25) Lee, Y. J.; Brandbyge, M.; Puska, M. J.; Taylor, J.; Stokbro, K.; Nieminen, R. M. Electron transport through monovalent atomic wires. *Phys. Rev. B* **2004**, *69*, No. 125409.
(26) García-Suárez, V. M.; Manrique, D. Z.; Lambert, C. J.; Ferrer, J. Anisotropic magnetoresistance in atomic chains of iridium and platinum from first principles. *Phys. Rev. B* **2009**, *79*, No. 060408.
(27) Chen, X. C.; Yang, J.; Zhou, Y. H.; Xu, Y. First-principles calculation of the transport properties of silicon-carbon (Si-C) and alumium-nitrogen (Al-N) nanowires. *Acta Phys. Sin.* **2009**, *58*, 3064−3070.
(28) Yu, J. X.; Cheng, Y.; Sanvito, S.; Chen, X. R. Bias-dependent oscillatory electron transport of monatomic sulfur chains. *Appl. Phys. Lett.* **2012**, *100*, No. 103110.
(29) Li, L. H.; Li, C. P.; Chen, Y. Synthesis of boron nitride nanotubes, bamboos and nanowires. *Phys. E* **2008**, *40*, 2513−2516.
(30) Chen, Y. J.; Chi, B.; Mahon, D. C.; Chen, Y. An effective approach to grow boron nitride nanowires directly on stainless-steel substrates. *Nanotechnology* **2006**, *17*, 2942−2946.
(31) Cretu, O.; Komsa, H. P.; Lehtinen, O.; Algara-Siller, G.; Kaiser, U.; Suenaga, K.; Krasheninnikov, A. V. Experimental observation of boron nitride chains. *ACS Nano* **2014**, *8*, 11950−11957.
(32) Rong, Y. M.; Warner, J. H. Wired up: interconnecting two-dimensional materials with one-dimensional atomic chains. *ACS Nano* **2014**, *8*, 11907−11912.
(33) Zhang, S.; Wang, Q.; Kawazoe, Y.; Jena, P. Three-dimensional metallic boron nitride. *J. Am. Chem. Soc.* **2013**, *135*, 18216−18221.
(34) Wang, S. L.; Yang, C. L.; Wang, M. S.; Ma, X. G. Electronic transport properties for molecules junctions of the three-dimensional BN and their sp3 bonded atoms substituted by P or Al atom. *J. Ludong Univ.: Nat. Sci. Ed.* **2017**, *33*, 26−30.
(35) Wang, S. L.; Yang, C. L.; Wang, M. S.; Ma, X. G.; Xin, J. G. Negative differential resistance and switch behavior of T-BxNy(x, y= 5, 6, 11) molecular junctions. *Phys. Lett. A* **2017**, *381*, 1493−1497.
(36) Zeng, J.; Chen, K. Q.; Deng, Y. X. Electron transport properties of boron nitride chains between two-dimensional metallic borophene electrodes. *Phys. E* **2019**, *114*, No. 113565.
(37) Xu, X.; Li, W.; Liu, L.; Feng, J.; Jiang, Y.; Tian, W. Q. Implementation of outstanding Electronic transport in polar covalent boron nitride atomic chains: another extraordinary odd-even behaviour. *Sci. Rep.* **2016**, *6*, No. 26389.
(38) Kohn, W.; Sham, L. J. Self-Consistent Equations Including Exchange And Correlation Effects. *Phys. Rev.* **1965**, *140*, A1133−A1138.
(39) Jauho, A. P.; Wingreen, N. S.; Meir, Y. Time-dependent transport in interacting and noninteracting resonant-tunneling systems. *Phys. Rev. B* **1994**, *50*, 5528−5544.
(40) Levendorf, M.; Kim, C. J.; Brown, L.; Huang, P.; Havener, R.; Muller, D.; Park, J. Graphene and boron nitride lateral hetero-structures for atomically thin circuitry. *Nature* **2012**, *488*, 627−632.
(41) Sutter, P.; Cortes, R.; Lahiri, J.; Sutter, E. Interface formation in monolayer graphene-boron nitride heterostructures. *Nano Lett.* **2012**, *12*, 4869−4874.
(42) Fan, X. F.; Shen, Z. X.; Liu, A. Q.; Kuo, J. L. Band gap opening of graphene by doping small boron nitride domains. *Nanoscale* **2012**, *4*, 2157−2165.
(43) Cahangirov, S.; Topsakal, M.; Ciraci, S. Long-range interactions in carbon atomic chains. *Phys. Rev. B* **2010**, *82*, No. 195444.
(44) D'yachkov, P. N.; Zaluev, V. A.; Piskunov, S. N.; Zhukovskii, Y. F. Comparative analysis of the electronic structures of mono- and bi-atomic chains of IV, III−V and II−VI group elements calculated using the DFT LCAO and LACW methods. *RSC Adv.* **2015**, *5*, 91751−91759.
(45) Senger, R. T.; Tongay, S.; Durgun, E.; Ciraci, S. Atomic chains of group-IV elements and III-V and II-VI binary compounds studied by a first-principles pseudopotential method. *Phys. Rev. B* **2005**, *72*, No. 075419.
(46) Abdurahman, A.; Shukla, A.; Dolg, M. Ab initiomany-body calculations on infinite carbon and boron-nitrogen chains. *Phys. Rev. B* **2002**, *65*, No. 115106.
(47) Shi, X. Q.; Dai, Z. X.; Zheng, X. H.; Zeng, Z. Ab initio electron transport study of carbon and boron-nitrogen nanowires. *J. Phys. Chem. B* **2006**, *110*, 16902−16907.

https://doi.org/10.1021/acsomega.1c00999
ACS Omega 2021, 6, 15727−15736

(48) Yu, J. X.; Hou, Z. W.; Liu, X. Y. Stability of conductance oscillations in carbon atomic chains. *Chin. Phys. B* **2015**, *24*, No. 067307.
(49) Crljen, Ž.; Baranović, G. Unusual Conductance of Polyyne-Based Molecular Wires. *Phys. Rev. Lett.* **2007**, *98*, No. 116801.
(50) Mu, Y.; Zeng, Z. Y.; Cheng, Y.; Chen, X. R. Electronic transport properties of silicon carbide molecular junctions: first-principles study. *RSC Adv.* **2016**, *6*, 91453−91462.
(51) Kristensen, I. S.; Mowbray, D. J.; Thygesen, K. S.; Jacobsen, K. W. Comparative study of anchoring groups for molecular electronics: structure and conductance of Au-S-Au and Au-NH2-Au junctions. *J. Phys.: Condens. Matter* **2008**, *20*, No. 374101.
(52) Liu, F. T.; Zhang, S. H.; Cheng, Y.; Chen, X. R.; Cheng, X. H. Theoretical calculation of electron transport properties of atomic chains of (GaAs)n (n=1-4). *Acta. Phys. Sin.* **2016**, *65*, No. 106201.
(53) Liu, F. T.; Cheng, Y.; Cheng, X. H.; Yang, F. B.; Chen, X. R. Electron transport through a silicon atomic chain. *Chin. Phys. Lett.* **2013**, *30*, No. 067302.
(54) He, J.; Chen, F.; Li, J.; Sankey, O. F.; Terazono, Y.; Herrero, C.; Gust, D.; Moore, T. A.; Moore, A. L.; Lindsay, S. M. Electronic decay constant of carotenoid polyenes from single-molecule measurements. *J. Am. Chem. Soc.* **2005**, *127*, 1384−1385.
(55) Luo, L.; Choi, S. H.; Frisbie, C. D. Probing hopping conduction in conjugated molecular wires connected to metal electrodes. *Chem. Mater.* **2011**, *23*, 631−645.
(56) Sedghi, G.; Sawada, K.; Esdaile, L. J.; Hoffmann, M.; Anderson, H. L.; Bethell, D.; Haiss, W.; Higgins, S. J.; Nichols, R. J. Single molecule conductance of porphyrin wires with ultralow attenuation. *J. Am. Chem. Soc.* **2008**, *130*, 8582−8583.
(57) Li, X.; He, J.; Hihath, J.; Xu, B.; Lindsay, S. M.; Tao, N. Conductance of single alkanedithiols: conduction mechanism and effect of molecule-electrode contacts. *J. Am. Chem. Soc.* **2006**, *128*, 2135−2141.
(58) Su, T. A.; Li, H.; Klausen, R. S.; Kim, N. T.; Neupane, M.; Leighton, J. L.; Steigerwald, M. L.; Venkataraman, L.; Nuckolls, C. Silane and germane molecular electronics. *Acc. Chem. Res.* **2017**, *50*, 1088−1095.
(59) Nguyen, Q. V.; Martin, P.; Frath, D.; Della Rocca, M. L.; Lafolet, F.; Bellinck, S.; Lafarge, P.; Lacroix, J. C. Highly efficient long-range electron transport in a viologen-based molecular junction. *J. Am. Chem. Soc.* **2018**, *140*, 10131−10134.
(60) Yao, X.; Sun, X.; Lafolet, F.; Lacroix, J. C. Long-range charge transport in diazonium-based single-molecule junctions. *Nano Lett.* **2020**, *20*, 6899−6907.
(61) Van Nguyen, Q.; Tefashe, U.; Martin, P.; Della Rocca, M. L.; Lafolet, F.; Lafarge, P.; McCreery, R. L.; Lacroix, J.-C. Molecular signature and activationless transport in cobalt-terpyridine-based molecular junctions. *Adv. Electron. Mater.* **2020**, *6*, No. 1901416.
(62) Dai, Z. X.; Zheng, X. H.; Shi, X. Q.; Zeng, Z. Effects of contact geometry on transport properties of a Si4 cluster. *Phys. Rev. B* **2005**, *72*, No. 205408.
(63) Fu-Ti, L..; Cheng, Y.; Chen, X. R.; Cheng, X. H.; Zeng, Z. Q. Theoretical calculation of electron transport properties of the Au-Si60-Au molecular junctions. *Acta Phys. Sin.* **2014**, *63*, No. 177304.
(64) Staykov, A.; Nozaki, D.; Yoshizawa, K. Theoretical study of donor-pi-bridge-acceptor unimolecular electric rectifier. *J. Phys. Chem. C* **2007**, *111*, 11699−11705.
(65) Seminario, J. M.; Zacarias, A. G.; Derosa, P. A. Theoretical analysis of complementary molecular memory devices. *J. Phys. Chem. A* **2001**, *105*, 791−795.
(66) Yuan, S. D.; Wang, S. Y.; Mei, Q. B.; Ling, Q. D.; Wang, L. H.; Huang, W. First-principles study of rectification in bis-2-(5-ethynylthienyl)ethyne molecular junctions. *J. Phys. Chem. A* **2011**, *115*, 9033−9042.
(67) Ke, S.-H.; Baranger, H. U.; Yang, W. Electron transport through single conjugated organic molecules: Basis set effects in ab initio calculations. *J. Chem. Phys.* **2007**, *127*, No. 144107.
(68) Mu, Y.; Zhou, Y.; Zhang, T.; Zeng, Z.-Y.; Cheng, Y. Electronic transport of (SiC)n (n = 1−4) molecular chains via first-principles calculations. *J. Chem. Eng. Data* **2017**, *62*, 3889−3902.
(69) SenthilKannan, K.; Sivaramakrishnan, V.; Kalaipoonguzhali, V.; Chinnadurai, M.; Kannan, S. Electronic transport, HOMO−LUMO and computational studies of CuS monowire for nano device fabrication by DFT approach. *Mater. Today: Proc.* **2020**, *33*, 2746−2749.
(70) Nguyen, Q. V.; Martin, P.; Frath, D.; Della Rocca, M. L.; Lafolet, F.; Barraud, C.; Lafarge, P.; Mukundan, V.; James, D.; McCreery, R. L.; Lacroix, J.-C. Control of rectification in molecular junctions: contact effects and molecular signature. *J. Am. Chem. Soc.* **2017**, *139*, 11913−11922.
(71) Chen, W.; Chen, Z.; Zheng, S. The influence of driving force on intramolecular electron transfer: A theoretical study of subphthalocyanine-AzaBODIPY-C60 supramolecular triad. *Int. J. Quantum Chem.* **2020**, *120*, No. e26131.
(72) Pan, J. B.; Zhang, Z. H.; Ding, K. H.; Deng, X. Q.; Guo, C. Current rectification induced by asymmetrical electrode materials in a molecular device. *Appl. Phys. Lett.* **2011**, *98*, No. 092102.
(73) Chen, X.; Roemer, M.; Yuan, L.; Du, W.; Thompson, D.; del Barco, E.; Nijhuis, C. A. Molecular diodes with rectification ratios exceeding 105 driven by electrostatic interactions. *Nat. Nanotechnol.* **2017**, *12*, 797−803.
(74) Zhang, Y. Y.; Wang, F. C.; Zhao, Y. P. Negative differential resistance behavior of silicon monatomic chain encapsulated in carbon nanotubes. *Comput. Mater. Sci.* **2012**, *62*, 87−92.
(75) Wan, H. Q.; Xu, Y. Dual conductance, negative differential resistance, and rectifying behavior in a molecular device modulated by side groups. *J. Chem. Phys.* **2012**, *136*, No. 184704.
(76) Kaur, M.; Sawhney, R. S.; Engles, D. Non-equilibrium tunneling through Au-C20-Au molecular bridge using density functional theory-non-equilibrium Green function approach. *J. Mater. Res.* **2016**, *31*, 2025−2034.
(77) Ke, S. H.; Baranger, H. U.; Yang, W. T. Models of electrodes and contacts in molecular electronics. *J. Chem. Phys.* **2005**, *123*, No. 114701.
(78) Taylor, J.; Guo, H.; Wang, J. Ab initio modeling of quantum transport properties of molecular electronic devices. *Phys. Rev. B* **2001**, *63*, No. 245407.
(79) Troullier, N.; Martins, J. L. Efficient pseudopotentials for plane-wave calculations. *Phys. Rev. B* **1991**, *43*, 1993−2006.
(80) Khoo, K. H.; Neaton, J. B.; Son, Y. W.; Cohen, M. L.; Louie, S. G. Negative differential resistance in carbon atomic wire-carbon nanotube junctions. *Nano Lett.* **2008**, *8*, 2900−2905.
(81) Perdew, J. P.; Zunger, A. Self-interaction correction to density-functional approximations for many-electron systems. *Phys. Rev. B* **1981**, *23*, 5048−5079.
(82) Shen, L.; Zeng, M. G.; Yang, S. W.; Zhang, C.; Wang, X. F.; Feng, Y. P. Electron transport properties of atomic carbon nanowires between graphene electrodes. *J. Am. Chem. Soc.* **2010**, *132*, 11481−11486.
(83) Brandbyge, M.; Mozos, J. L.; Ordejon, P.; Taylor, J.; Stokbro, K. Density-functional method for nonequilibrium electron transport. *Phys. Rev. B* **2002**, *65*, No. 165401.
(84) Ordejon, P. Linear scaling ab initio calculations in nanoscale materials with SIESTA. *Phys. Status Solidi B* **2000**, *217*, 335−356.
(85) Ying, C.; Hu, H. F.; Wang, X. W.; Zhang, Z. J.; Cheng, C. P. Rectifying behaviors induced by B/N-doping in similar right triangle graphene devices. *Acta. Phys. Sin.* **2015**, *64*, No. 196101.
(86) Büttiker, M.; Imry, Y.; Landauer, R.; Pinhas, S. Generalized many-channel conductance formula with application to small rings. *Phys. Rev. B* **1985**, *31*, 6207−6215.

https://doi.org/10.1021/acsomega.1c00999
ACS Omega 2021, 6, 15727−15736